

Cellulose defects in the Arabidopsis secondary cell wall promote early chloroplast development

Duorong Xu¹ , Ravi Dhiman¹, Adriana Garibay², Hans-Peter Mock², Dario Leister¹ and Tatjana Kleine^{1,*} 

¹Plant Molecular Biology, Faculty of Biology, Ludwig-Maximilians University of Munich, Großhaderner Str. 2, 82152, Planegg-Martinsried, Germany, and

²Department of Physiology and Cell Biology, Leibniz Institute of Plant Genetics and Crop Plant Research (IPK-Gatersleben), Corrensstraße 3, 06466, Stadt Seeland, OT Gatersleben, Germany

Received 15 May 2019; revised 12 August 2019; accepted 28 August 2019; published online 9 September 2019.

*For correspondence (e-mail tatjana.kleine@lmu.de).

SUMMARY

Lincomycin (LIN)-mediated inhibition of protein synthesis in chloroplasts prevents the greening of seedlings, represses the activity of photosynthesis-related genes in the nucleus, including *LHCB1.2*, and induces the phenylpropanoid pathway, resulting in the production of anthocyanins. In *genomes uncoupled* (*gun*) mutants, *LHCB1.2* expression is maintained in the presence of LIN or other inhibitors of early chloroplast development. In a screen using concentrations of LIN lower than those employed to isolate *gun* mutants, we have identified *happy on lincomycin* (*holi*) mutants. Several *holi* mutants show an increased tolerance to LIN, exhibiting de-repressed *LHCB1.2* expression and chlorophyll synthesis in seedlings. The mutations responsible were identified by whole-genome single-nucleotide polymorphism (SNP) mapping, and most were found to affect the phenylpropanoid pathway; however, *LHCB1.2* expression does not appear to be directly regulated by phenylpropanoids, as indicated by the metabolic profiling of mutants. The most potent *holi* mutant is defective in a subunit of cellulose synthase encoded by *IRREGULAR XYLEM 3*, and comparative analysis of this and other cell-wall mutants establishes a link between secondary cell-wall integrity and early chloroplast development, possibly involving altered ABA metabolism or sensing.

Keywords: chloroplast, lincomycin, retrograde signaling, cell wall, phenylpropanoids.

INTRODUCTION

The vast majority of the several thousand proteins found in plastids are encoded by nuclear genes (Timmis *et al.*, 2004). As endosymbiotic descendants of cyanobacteria, however, plastids still contain 80–230 genes, most of which are involved in essential plastid functions like energy production and plastid gene expression (PGE) (Ponce-Toledo *et al.*, 2017). As a result, plastid multiprotein complexes (including the photosystems and ribosomes) consist of subunits encoded by both the nuclear and plastid genomes. This in turn accounts for the need for coordination of PGE and nuclear gene expression (NGE). Thus, the nucleus influences activity in the plastids, including PGE, via ‘anterograde control/signaling’ (Stern *et al.*, 2010), whereas plastids communicate their developmental and metabolic status to the nucleus via ‘retrograde signaling’, allowing the nucleus to adjust NGE appropriately (Kleine *et al.*, 2009; Chi *et al.*, 2013; Terry and Smith, 2013; Chan *et al.*, 2016; Kleine and Leister, 2016). Plastid-derived retrograde

signals can be divided into two classes: signals related to the operation of the plastid under changing environmental conditions (operational control) and signals triggered by changes in plastid and photosystem biogenesis (biogenic control) (Chan *et al.*, 2016).

Forward-genetic screens have permitted the identification of components involved in retrograde signaling pathways (Kleine and Leister, 2016). They have exploited the fact that the expression of nuclear genes for plastid proteins like *LHCB1.2* (a major light-harvesting chlorophyll *a/b*-binding protein) is reduced in seedlings exposed to inhibitors of PGE (e.g. lincomycin, LIN) or carotenoid biosynthesis (e.g. norflurazon, NF) (Oelmüller and Mohr, 1986; Oelmüller *et al.*, 1986). The first mutant screen specifically designed to characterize components of biogenic plastid signaling was performed with *Arabidopsis thaliana* seedlings grown on NF (Susek *et al.*, 1993), and identified mutant seedlings that continued to accumulate *LHCB1.2* transcripts. Five different *genomes uncoupled* (*gun*)

mutants were initially isolated (Susek *et al.*, 1993; Mochizuki *et al.*, 2001). *GUN1* codes for a nucleic-acid-binding chloroplast protein (Koussevitzky *et al.*, 2007), whereas *GUN2–GUN5* encode enzymes of the tetrapyrrole biosynthesis pathway (Mochizuki *et al.*, 2001; Larkin *et al.*, 2003). Subsequent investigations of the *gun* mutants led to contradictory conclusions as to a putative plastid signaling function of the tetrapyrrole pathway intermediate Mg-protoporphyrin IX (Strand *et al.*, 2003; Mochizuki *et al.*, 2008; Moulin *et al.*, 2008). To resolve these discrepancies, a gain-of-function screen based on activation tagging was conducted in the reporter line that was used in the original *gun* mutant screen (Woodson *et al.*, 2011). This screen identified the *gun6-1D* mutant, which overexpresses ferredoxin-NADP+ reductase 1 (FC1), and prompted the proposal that the tetrapyrrole heme – specifically the fraction produced by FC1 – might function as a biogenic retrograde signal (Woodson *et al.*, 2011; Terry and Smith, 2013). With the intention of identifying additional mutants with more subtle *gun* phenotypes than those detected in the original screen (Susek *et al.*, 1993), a transgenic line in which the *LHCB1.1* promoter was fused to the more sensitive reporter luciferase was used in a further screen (Ruckle *et al.*, 2007), and mutants that exhibited a *gun* phenotype on NF were also tested on LIN-containing medium. As a result, four *cryptochrome 1* (*cry1*) alleles and *long hypocotyl 5* (*hy5*) were identified (Ruckle *et al.*, 2007). More recently, overexpressors of GLK1 or GLK2 have been shown to behave like strong *gun* mutants when challenged with NF or LIN (Leister and Kleine, 2016; Martin *et al.*, 2016).

Inhibitors like NF and LIN have numerous secondary effects, however: for example, the massive accumulation of anthocyanins (Cottage *et al.*, 2010; Voigt *et al.*, 2010). A modified version of the *gun* mutant screen was therefore designed, which used less NF and a lower light intensity, and resulted in fewer side effects, primarily by avoiding anthocyanin accumulation (Saini *et al.*, 2011). Unlike the original *gun* mutants and wild-type (WT) plants, the *happy on norflurazon* (*hon*) mutants recovered in this screen remained green in the presence of (lower doses of) NF. The *hon* mutations were mapped to ClpR4, a nucleus-encoded subunit of the plastid-localized Clp protease complex, and to a putative chloroplast translation elongation factor, and thus are likely to interfere with PGE and plastid protein homeostasis (Saini *et al.*, 2011).

Lincomycin and NF have similar effects on *gun1*, *hy5* and *cry1* (Ruckle *et al.*, 2007) mutants, as well as on the GLK overexpressors (Leister and Kleine, 2016; Martin *et al.*, 2016), but *gun2*, *gun4* and *gun5* mutants differ in their responses to these agents (Gray *et al.*, 2003). This distinction suggests that NF and LIN trigger at least partially different signaling pathways.

In an effort to isolate additional *gun* mutants specifically for the LIN pathway(s), we screened an ethyl

methanesulfonate (EMS)-mutagenized *A. thaliana* Col-0 population grown in the presence of a greater than four-fold lower dose of LIN than that used in the earlier screens. In this way, *happy on lincomycin* (*holi*) mutants that are able to green in the presence of LIN were identified. In a second screen with a fivefold lower NF concentration relative to that used in the original screens, we identified additional *hon* mutants. Characterization of these mutants suggested that: (i) there is no correlation between *gun* signaling and anthocyanin biosynthesis; and (ii) early chloroplast development is linked to cell-wall integrity.

RESULTS

Isolation of *happy on lincomycin* (*holi*) mutants

Seedlings grown on LIN experience severe photo-oxidative damage, plastid biogenesis is arrested at a proplastid-like stage, even under normal light conditions (Oelmüller and Mohr, 1986), and the expression of nuclear genes encoding chloroplast proteins is altered (Oelmüller *et al.*, 1986). In screens intended to isolate mutants displaying the *gun* phenotype on LIN, a concentration of 220 µg ml⁻¹ LIN (high LIN) and light intensities of 100–125 µmol photons m⁻² sec⁻¹ were used (Koussevitzky *et al.*, 2007; Ruckle *et al.*, 2007). Under such conditions, 5-day-old *A. thaliana* Col-0 seedlings were retarded in growth, failed to green and accumulated appreciable concentrations of anthocyanins (Figure 1a). Using the same light intensity as in previous screens, we gradually reduced the LIN concentration until the coloration of the seedling population turned from purple (as a result of anthocyanin production) to greenish or white. Although some seedlings turned light green with a concentration of 25 µg ml⁻¹ LIN, growth on 50 µg ml⁻¹ LIN (low LIN) produced uniformly purple-colored seedlings (Figure 1a). The latter concentration was still sufficient to reduce the accumulation of the nucleus-encoded transcripts encoding the chloroplast proteins Lhcb1.2 and CA1 to 8.0% (high LIN, 1.5%) and 6% (high LIN, 1.0%), respectively, of the levels seen in MS-grown seedlings (Figure 1b). Thus, this low LIN dose still activates retrograde signaling. The *gun1-1* mutant used as a control accumulated fewer anthocyanins than the WT when grown on high LIN, confirming a previous finding (Cottage *et al.*, 2010). Approximately half of the *gun1-1* seedlings grown on low LIN displayed whitish cotyledons, which were larger than those of the WT (Figure 1a).

Based on these observations, a screen was set up to identify mutants with an altered, visually discernible phenotype on low LIN. To this end, Col-0 seeds were mutagenized with EMS. The M₁ plants were grown to maturity to produce M₂ seeds, and ~20 000 4- to 5-day-old M₂ seedlings were grown on low LIN and screened for alterations in the color or size of cotyledons. This led to the isolation of six *holi* mutants (Figure 2). The mutants *holi1* and *holi3*

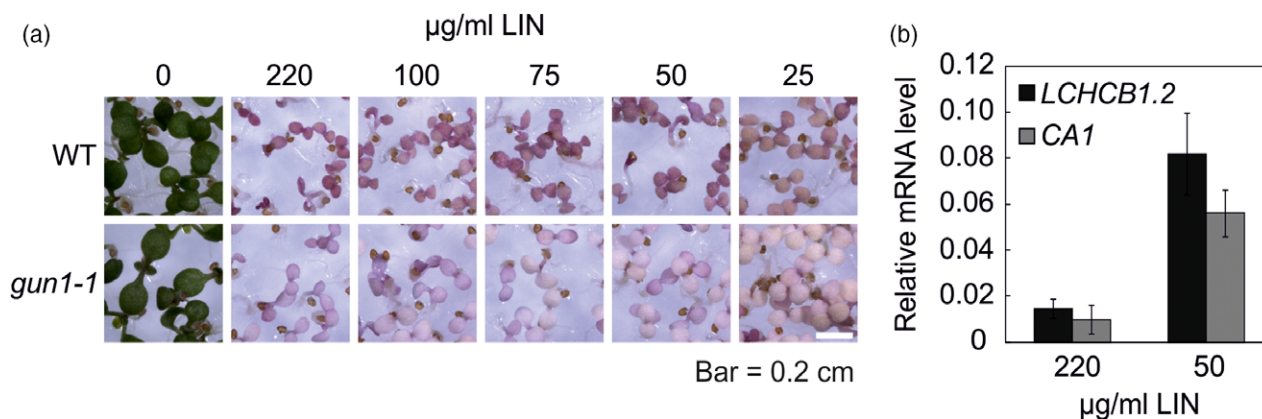


Figure 1. Effects of different lincomycin (LIN) doses on seedling development and nuclear transcript levels. (a) Pictures of wild-type (WT) and *gun1-1* seedlings grown for 5 days on MS supplemented with the indicated concentrations of LIN. (b) Quantitative reverse-transcriptase PCR was used to determine *LHCb1.2* and *CA1* mRNA levels in WT seedlings grown under continuous light ($100 \mu\text{mol photons m}^{-2} \text{sec}^{-1}$) on MS plates without inhibitor or supplemented with either $50 \mu\text{g ml}^{-1}$ LIN or $220 \mu\text{g ml}^{-1}$ LIN. The levels of *LHCb1.2* and *CA1* mRNA are expressed relative to those in the WT control (grown in the absence of inhibitor), which was set to 1. The results were normalized to the expression level of *AT4G36800*. Mean values were derived from two independent experiments, each with three technical replicates. Error bars indicate standard deviations.

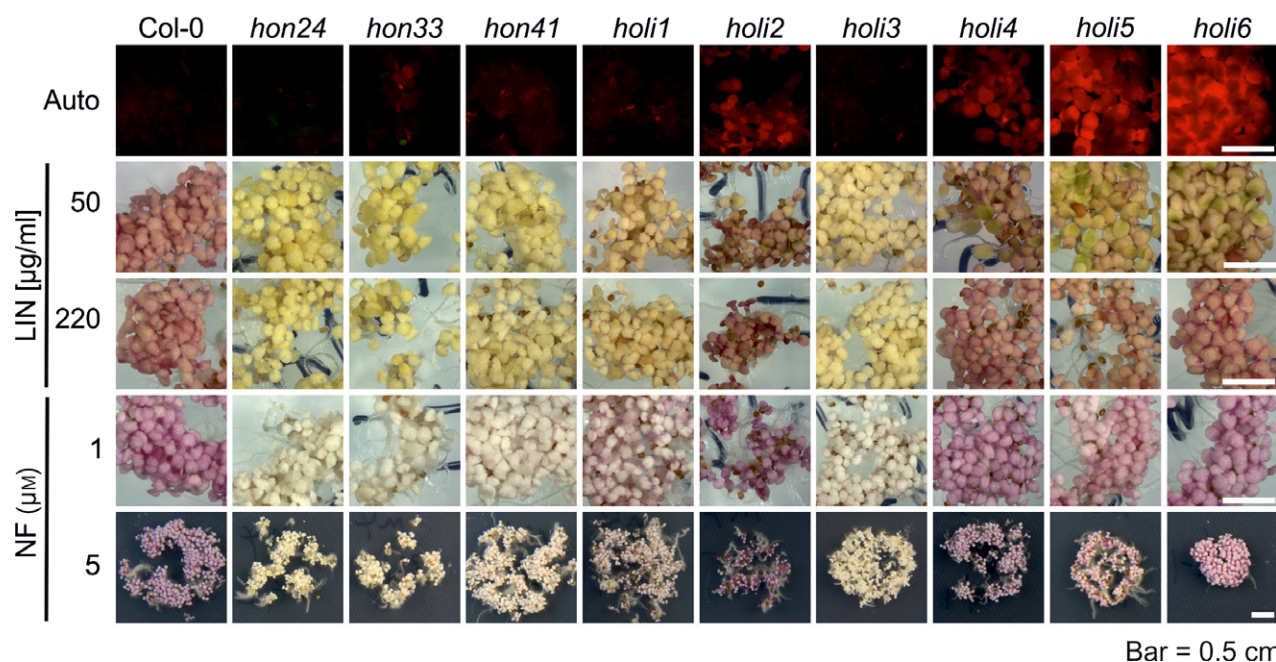


Figure 2. Phenotypes of identified *holi* and *hon* mutants grown in the presence of lincomycin (LIN) or norflurazon (NF). Wild-type (WT), *holi* and *hon* mutant seedlings were grown for 5 days under continuous light ($100 \mu\text{mol photons m}^{-2} \text{sec}^{-1}$) on MS plates supplemented with either LIN (50 or $220 \mu\text{g ml}^{-1}$) or NF (1 or $5 \mu\text{M}$). Autofluorescence after UV excitation was monitored in seedlings grown on MS plates supplemented with $50 \mu\text{g ml}^{-1}$ LIN. The red autofluorescence was used as an indicator for chlorophyll accumulation.

had yellowish cotyledons and did not accumulate anthocyanins. Cotyledons of the other mutants turned light green and accumulated anthocyanins to various levels. When grown on high levels of LIN, *holi2* displayed smaller cotyledons and hyperaccumulation of anthocyanins compared with all other mutants and the WT (Figure 2). A similar screen in which low LIN was replaced by low NF ($1 \mu\text{M}$, instead of the $5 \mu\text{M}$ NF used in the original *gun* mutant

screen; Susek *et al.*, 1993) aimed to identify new *hon* mutants. This screen yielded *hon* mutants (*hon24*, *hon33* and *hon41*) with completely white cotyledons. On low LIN, the cotyledons of these *hon* mutants also appeared yellow-greenish, like those of the *holi* mutants (Figure 2). To confirm that the greenish color was caused by chlorophyll accumulation, autofluorescence was monitored after UV excitation of seedlings grown on low LIN (Figure 2). Col-0,

holi3 and *hon24* seedlings displayed no autofluorescence, as expected when chlorophyll is absent; however, four mutants (*holi2*, *holi14*, *holi5* and *holi6*) displayed marked levels of autofluorescence, whereas three others (*holi1*, *hon33* and *hon41*) displayed weaker autofluorescence. Notably, none of the *hon* or *holi* mutants appeared greener on either high or low NF (Figure 2), in agreement with the absence of chlorophyll autofluorescence observed under these conditions.

Several *holi* mutants display a *gun* phenotype on low LIN

The chlorophyll-autofluorescence phenotype of some of the *hon* and *holi* mutants prompted us to test whether their continued plastid development despite growth on LIN was associated with altered signaling to the nucleus. To this end, RNA was prepared from 5-day-old Col-0, *gun1-1*, and the various *hon* and *holi* mutant seedlings grown on low LIN, and subjected to Northern analysis to determine the steady-state levels of *LHCB1.2* mRNA. Following exposure to the low LIN concentration, the *gun1-1* mutant showed, as expected, higher *LHCB1.2* mRNA expression than the WT (Figure 3). Remarkably, *LHCB1.2* mRNA levels in the *holi2*, *holi4*, *holi5* and *holi6* mutants were comparable with, or even higher than, that of the *gun1-1* mutant. Under control conditions (without inhibitor treatment), however, *LHCB1.2* mRNA levels were already slightly elevated in the *holi2*, *holi3*, *holi5* and *holi6* mutants, which means that the *gun* phenotype on low LIN was relativized by around 1.7-fold (Figure 3). Grown on low NF, some of the *holi* mutants also displayed very weak *gun* phenotypes. But none of the identified *hon* and *holi* mutants behaved like a *gun* mutant when grown on high NF or high LIN (Figure 3).

The majority of *HOLI* and *HON* loci encode proteins involved in the flavonoid pathway

In order to explain the ability of some of the identified mutants to accumulate chlorophyll and maintain *LHCB1.2* transcript accumulation in the presence of low LIN, the M₄ generation of the mutant plants was back-crossed to their parent Col-0, and seedlings displaying recessive and semi-dominant (in the case of *holi2*) mutant phenotypes were identified in the F₂ generation. The underlying mutations were localized by next-generation sequencing (see Experimental procedures) and confirmed by Sanger sequencing. The *holi1* and *hon41* mutations turned out to be allelic, and both were mapped to the gene for the transcription factor MYB DOMAIN PROTEIN 75 (MYB75; PRODUCTION OF ANTHOCYANIN PIGMENT 1, PAP1). The C→T substitution at nucleotide (nt) 902 (relative to the start codon, as also in the following) in *holi1* results in the replacement of an Arg by an Lys residue and permits some anthocyanin accumulation, whereas in *hon41* a C→T substitution at nt 39 introduces a stop codon in the first exon (Figure 4), completely blocking anthocyanin accumulation (Figure 2).

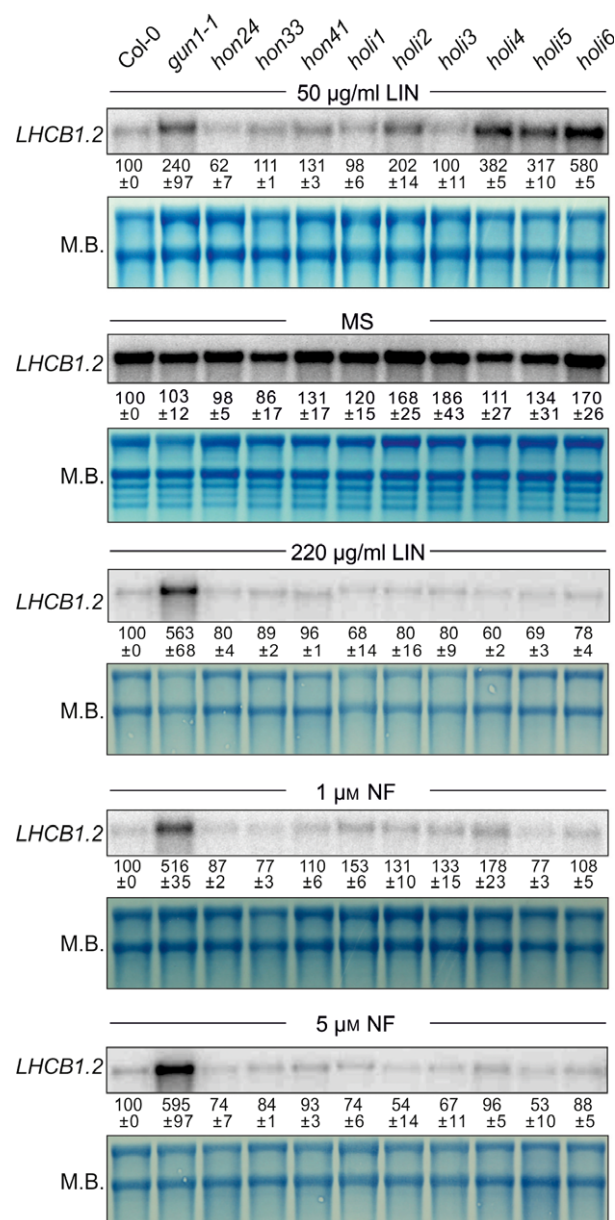


Figure 3. *LHCB1.2* transcript levels found in WT, *gun1-1*, *holi* and *hon* mutant seedlings grown without inhibitor or in the presence of lincomycin (LIN) or norflurazon (NF). Seedlings were grown for 5 days under continuous light (100 µmol photons m⁻² sec⁻¹) on MS plates without inhibitor or supplemented with either LIN (50 or 220 µg ml⁻¹) or NF (1 or 5 µM). *LHCB1.2* mRNA levels were determined by Northern blot analyses. The methylene blue-stained blots served as loading controls (M.B.).

Moreover, in *holi3* a Trp codon is replaced by a stop in the gene for the transcription factor TRANSPARENT TESTA GLABRA 1 (TTG1, required for purple anthocyanin accumulation). The G→A substitution at nt 10 in *hon24* and the C→T substitution at nt 987 in *hon33* caused non-sense mutations in DIHYDROFLAVONOL 4-REDUCTASE (DFR; TRANSPARENT TESTA 3, TT3) and ANTHOCYANIN

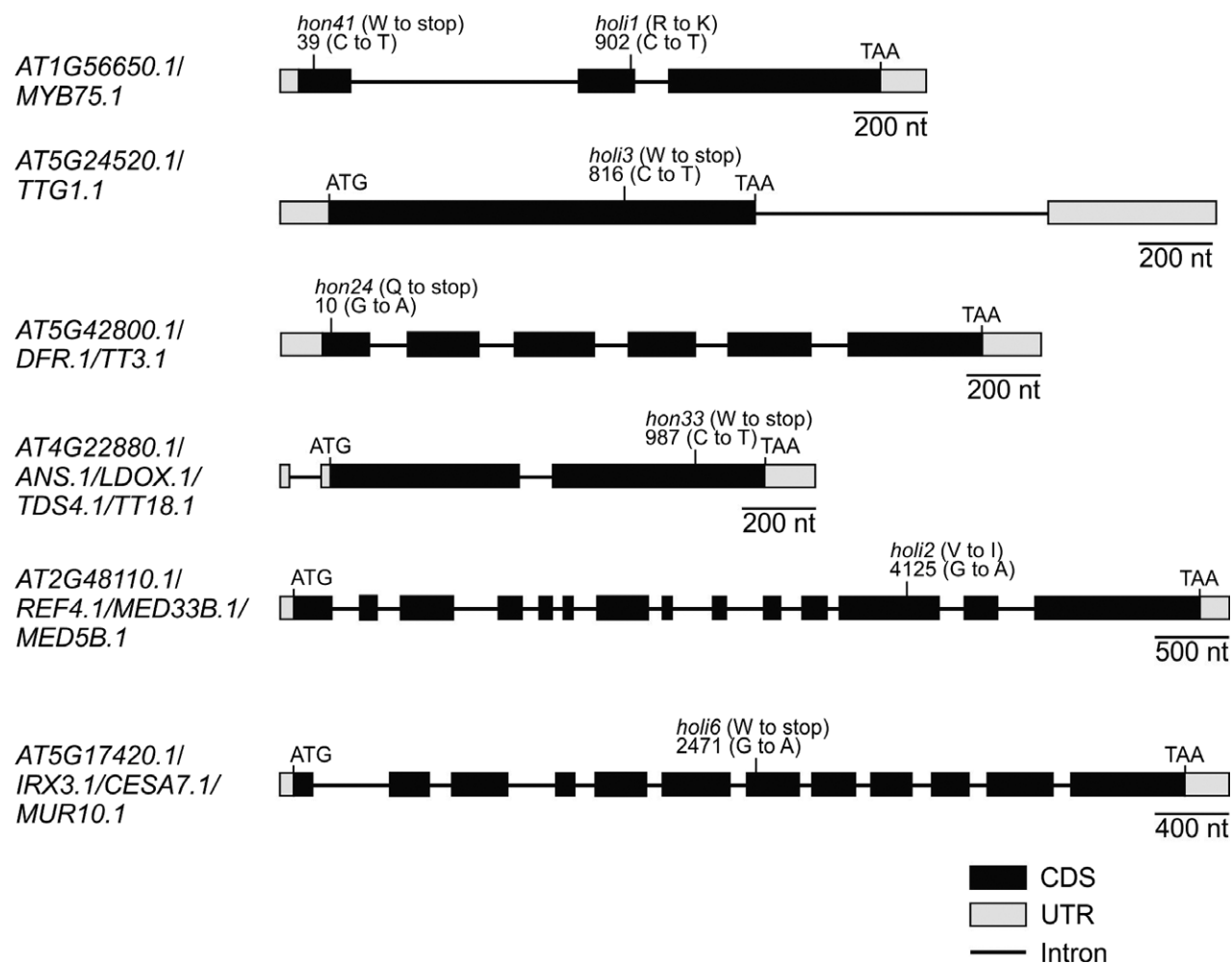


Figure 4. Schematic representation of the positions of identified *HOLI* and *HON* mutation sites. Exons (black boxes), introns (black lines), and the 5' and 3' untranslated regions (UTRs; grey boxes) are shown. Numbers are given relative to the start codon ATG.

SYNTHASE (ANS; LEUCOANTHOCYANIDIN DIOXYGENASE, LDOX; TANNIN DEFICIENT SEED 4, TDS4; TT18), respectively. The mutation that most probably causes the *holi2* mutant phenotype is located at nt 4125, and replaces a Val by an Ile residue in *REDUCED EPIDERMAL FLUORESCENCE 4* (*REF4*; *MEDIATOR COMPLEX MED 5B*, *MED5B*; *MED33B*). The G→A substitution in *holi6* introduces a premature stop in exon 7 of *IRREGULAR XYLEM 3* (*IRX3*; *CELLULOSE SYNTHASE 7*, *CESA7*; *MURUS 10*, *MUR10*). The mutations responsible for the *holi4* and *holi5* phenotypes could not be identified. With the exception of *IRX3*, all affected proteins have previously been shown to be involved in phenylpropanoid metabolism (Figure S1; Stout *et al.*, 2008; Appelhagen *et al.*, 2014). *MYB75* and *TTG1* are transcription factors, and *DFR* and *ANS* are enzymes that convert dihydroquercetin to leucocyanidin (*DFR*) and leucocyanidin to cyanidin, respectively (Figure S1). *REF4* is required for phenylpropanoid homeostasis and has been shown to interact directly with the conserved

transcriptional coregulatory complex Mediator (Bonawitz *et al.*, 2012).

Disturbances in the phenylpropanoid pathway do not confer a *gun* phenotype

Anthocyanins are produced via the flavonoid pathway, which is a branch of the general phenylpropanoid biosynthetic pathway (Tohge *et al.*, 2005; Appelhagen *et al.*, 2014). The *gun1-1* mutant clearly accumulates less anthocyanin than the WT when grown on both low and high LIN concentrations (Figure 1a), and it was noted previously that *gun2*, *gun4* and *gun5* mutants accumulate less anthocyanin than WT plants when grown on high NF (Voigt *et al.*, 2010). Therefore, the growth of 5-day-old *gun1*, *gun4* and *gun5* mutant seedlings was also tested under our reduced inhibitor conditions (Figure S2). In the WT, *gun1-1* and *gun1-102* seedlings, anthocyanin accumulation was clearly discernible in seedlings grown on low and high NF in continuous white light; however, on high NF, the

stronger *gun1* allele (*gun1-102*) displayed slightly less anthocyanin accumulation than the weaker allele (*gun1-1*) (Figure S2). In contrast, *gun4-1* and *gun5-1* accumulated less anthocyanin on both NF concentrations, whereas they accumulated WT levels of anthocyanins on high LIN. It has previously been speculated that plastid signals that require GUN2–GUN5 might stimulate anthocyanin biosynthesis, although anthocyanin content and *LHCB1.2* mRNA accumulation in *gun* mutants are not strictly correlated (Voigt *et al.*, 2010). As these authors considered only the accumulation of visible anthocyanins, reverse-phase ultra-performance liquid chromatography (UPLC) was used to profile the accumulation of phenylpropanoids in 5-day-old Col-0, *gun1-1*, *gun2-1*, *gun4-1* and *gun5-1* seedlings grown on MS in the absence or presence of high NF or high LIN. In the WT, high NF and high LIN caused approximately 2.0- and 1.5-fold increases in the total phenylpropanoid content, respectively (Figure S3; Table S1). Total phenylpropanoids were similarly boosted in the *gun2-1*, *gun4-1* and *gun5-1* mutants, but in *gun1-1* they were approximately 1.5-fold induced after NF treatment and not induced at all by treatment with high LIN. A closer look at the accumulation of specific phenylpropanoid components revealed that the difference between *gun1-1* and the WT is mainly attributable to a lack of induction of kaempferol derivatives in *gun1-1* (Figure S3; Table S1). In particular, kaempferol 3-O-[6"-O-(rhamnosyl) glucoside] 7-O-rhamnoside (k3; see also Figure S1) was less effectively induced in all investigated *gun* mutants after NF treatment, as well as in *gun1-1* after LIN treatment; none of the other detected compounds showed any consistent alteration in the *gun* mutants relative to the WT (Figure S3; Table S1). Levels of k3 are also reduced in the UDP-glucosyl transferase *ugt78d1 ugt78d2* mutant (Yin *et al.*, 2014). To definitively clarify whether disturbances in the phenylpropanoid pathway are linked to chloroplast development and/or a *gun* phenotype in the presence of inhibitors, 5-day-old *ugt78d1 ugt78d2* mutants, together with mutants impaired in enzymatic steps of the general phenylpropanoid pathway (Figure S1), or regulatory factors of flavonoid biosynthesis and transporters involved in proanthocyanidin accumulation (Appelhaugen *et al.*, 2014), were first tested for chlorophyll autofluorescence on low LIN (Figure 5). Because *cry1* mutants were previously identified as weak *gun* mutants on high LIN (Ruckle *et al.*, 2007), the mutants *cry1-304* and *cry1-304 cry2-1*, and the constitutive photomorphogenesis mutant *cop1-4*, were included as controls together with *gun1-1*. Chlorophyll autofluorescence could be detected in *gun1-1*, *cry1-304*, *cry1-304 cry2-1*, as well as in the *cop1-4* mutant (Figure 5). All transport-related and regulation mutants showed some chlorophyll fluorescence, although this was restricted to the hypocotyl in *ttg1-22*, *ttg2-5* and *tt8-6* mutants. The biosynthesis mutants

tt4-15, *tt5-2*, *tt7-7*, *tt3-1* and *tds4-2* showed the greenish fluorescence typical of kaempferol derivatives (Appelhaugen *et al.*, 2014) and only very weak or no chlorophyll autofluorescence (Figure 5). These mutants are defective in steps in the main pathway leading from chalcone synthase (*tt4-15*) to the conversion of leucocyanidin to cyanidin (*tds4-2*), which is the branch point for the production of anthocyanins and oxidized tannins (Figure S1). Thus, these mutants do not accumulate anthocyanins. The *ban-5*, *tt15-4*, *tt6-2* and *fls1-3* mutants displayed similar levels of chlorophyll fluorescence to the *gun1-1* and *cry1-304* mutants and the transport-related *aha10-6* mutant. The *tt10-8* mutant showed the strongest chlorophyll autofluorescence, which was reflected in a light greenish cotyledon phenotype, with some cotyledons even exhibiting a brighter green color (Figure 5).

When grown in the presence of low LIN or high NF, *gun1-1*, *cry1-304* and *cry1-304 cry2-1* seedlings accumulated *LHCB1.2* in the presence of the inhibitors but, in accordance with Ruckle *et al.* (2007), the *cop1-4* mutant did not (Figure 6a). It is noteworthy here that *cry1* and *cry1 cry2* seedlings grown on low LIN accumulated even higher levels of *LHCB1.2* mRNA than *gun1-1*. The *ugt78d1 ugt78d2* mutant (in which k3 is diminished) and the other phenylpropanoid mutants did not accumulate *LHCB1.2* mRNA, with the sole exception of the *tt10-8* mutant, which continued to express *LHCB1.2* in the presence of low LIN but not in the presence of high NF (Figure 6b). TT10/LAC15 is similar to laccase-like polyphenol oxidases and is involved in lignin biosynthesis (Liang *et al.*, 2006).

Taken together, these data imply that there is no direct link between phenylpropanoid accumulation and *gun* signaling.

A defect in the secondary cell wall promotes seedling greening

The *holi6* mutant was among the identified mutants that displayed the strongest chlorophyll autofluorescence when grown on MS plates supplemented with low LIN (Figure 2). To confirm that the premature stop in *IRX3* (*CESA7*) found in *holi6* was responsible for this phenotype, two additional *irx3* mutant alleles, *irx3-2* (confirmation of the T-DNA insertion and a lack of the full-length transcript is shown in Figure S4) and *irx3-4* (Brown *et al.*, 2005), were grown on low LIN. Indeed, the cotyledons of *irx3-2* and *irx3-4* were visibly greener and displayed higher autofluorescence than the cotyledons of the WT (Figure 7a), which is reflective of a higher chlorophyll content (Figure 7b). Moreover, although attempts to determine the maximum quantum yield of photosystem II (F_v/F_m) with an Imaging PAM fluorometer were unsuccessful in WT grown on low LIN, this parameter could be measured in *holi6*, and *irx3-2* and *irx3-4* displayed even higher F_v/F_m values (Figure 7a).

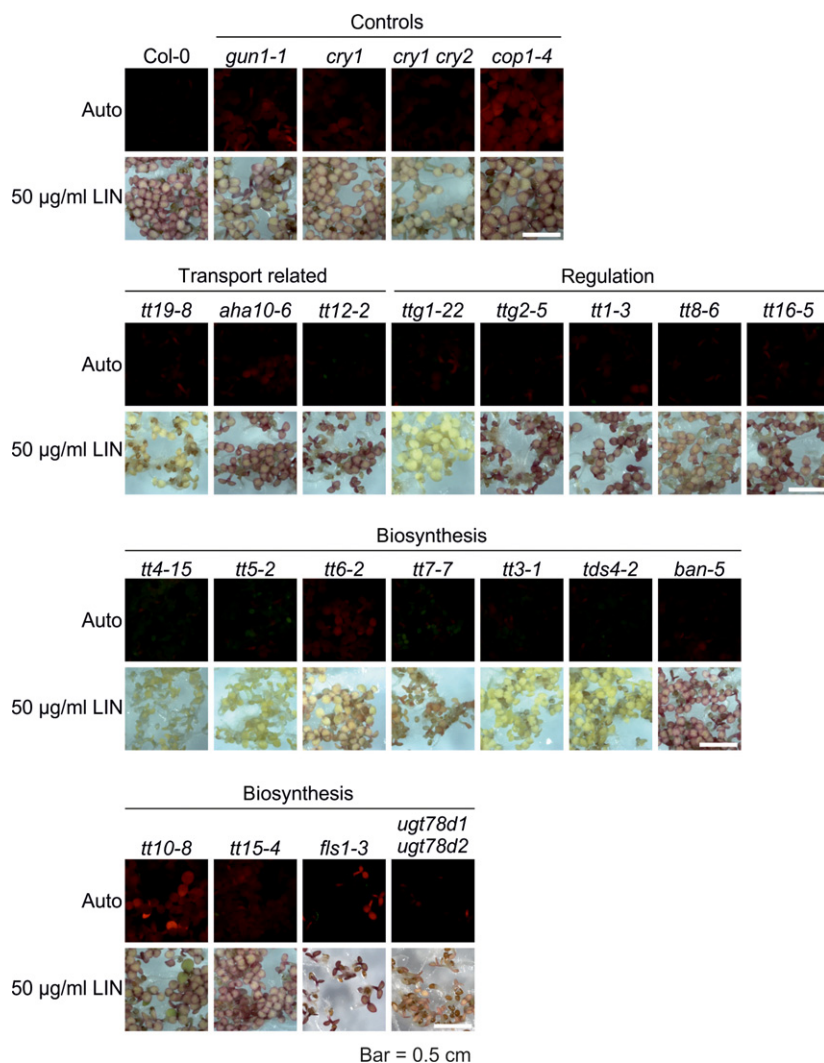


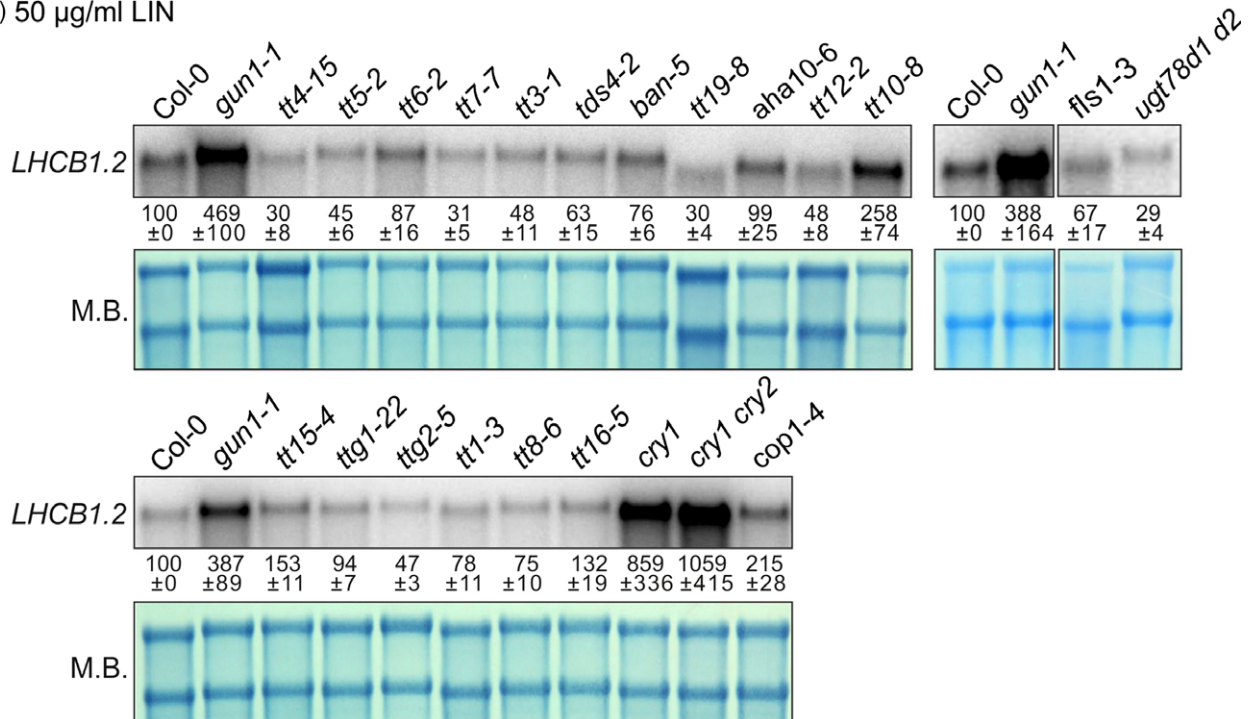
Figure 5. Phenotypes of the wild type (WT), *gun1*, *cry1*, *cry1 cry2*, *cop1-4* and mutants associated with phenylpropanoid biosynthesis grown on low lincomycin (LIN). WT, *gun1-1* and mutant seedlings with defects in the photomorphogenesis pathway (*cry1*, *cry1 cry2* and *cop1-4*), the biosynthesis pathway (*tt4-15*, *tt5-2*, *tt6-2*, *tt7-7*, *tt3-1*, *tds4-2*, *ban-5*, *tt10-8* and *tt15-4*), transport (*aha10-6*, *tt12-2* and *tt19-8*) and regulation (*ttg1-22*, *ttg2-5*, *tt1-3*, *tt8-6* and *tt16-5*) of various phenylpropanoids were grown for 5 days under continuous light ($100 \mu\text{mol photons m}^{-2} \text{sec}^{-1}$) on MS plates supplemented with $50 \mu\text{g ml}^{-1}$ LIN. Autofluorescence after UV excitation was monitored. The red fluorescence served as an indicator for chlorophyll accumulation.

IRX3/CESA7 is a member of the cellulose synthase (CESA) family. The CESA complexes required for the synthesis of primary and secondary cell walls differ in composition: IRX3, together with IRX1/CESA8 and IRX5/CESA4, is needed specifically for the synthesis of cellulose in the secondary cell wall, which also contains lignin (Meents *et al.*, 2018; Polko and Kieber, 2019). CESA1/RADIALLY SWOLLEN 1 (RSW1), CESA3 and CESA6-like proteins (CESA2, CESA5, CESA6 and CESA9) are involved in primary cell-wall synthesis (Meents *et al.*, 2018; Polko and Kieber, 2019).

These findings raise the question of whether the *holi* phenotype might be caused by: (i) a general reduction in cellulose content in the secondary cell wall; (ii) reduced cellulose content in the primary cell wall; or (iii) a lack of hemicelluloses in the secondary cell wall. To clarify this issue, mutants with reduced cellulose content in the secondary cell wall (*irx1-2*, *irx1-3* and *irx5-4*), together with a mutant with reduced cellulose content in the primary cell wall (*rsw1-1*; Williamson *et al.*, 2001) and a mutant with reduced content

of the hemicellulose xylan in the secondary cell wall (*irx9-2*; Bauer *et al.*, 2006), were germinated on low LIN medium. The *irx1* seedlings displayed comparably high autofluorescence to *holi6* seedlings, whereas *irx5-4* displayed weaker autofluorescence, and *rsw1-1* and *irx9-2* behaved like the WT (Figure 7c). Moreover, F_v/F_m could not be detected in the additionally investigated mutants. Reduced cellulose production can affect growth and morphogenesis in various plant parts, as exemplified by the swollen roots of *rsw1* mutants grown at 31°C (Arioli *et al.*, 1998; Williamson *et al.*, 2001). To test for any temperature dependency of the F_v/F_m phenotype, *rsw1-1* together with the other cell wall mutants was germinated at 31°C on control MS plates and on MS plates supplemented with low LIN. Cotyledons of the *rsw1-1* mutant were smaller under both conditions, confirming the heat growth phenotype observed previously (Williamson *et al.*, 2001), but, as in all other tested mutants, F_v/F_m was WT-like (Figure S5a). Interestingly, both the greening and the elevated F_v/F_m phenotypes were barely detectable under low LIN

(a) 50 µg/ml LIN



(b) 5 µM NF

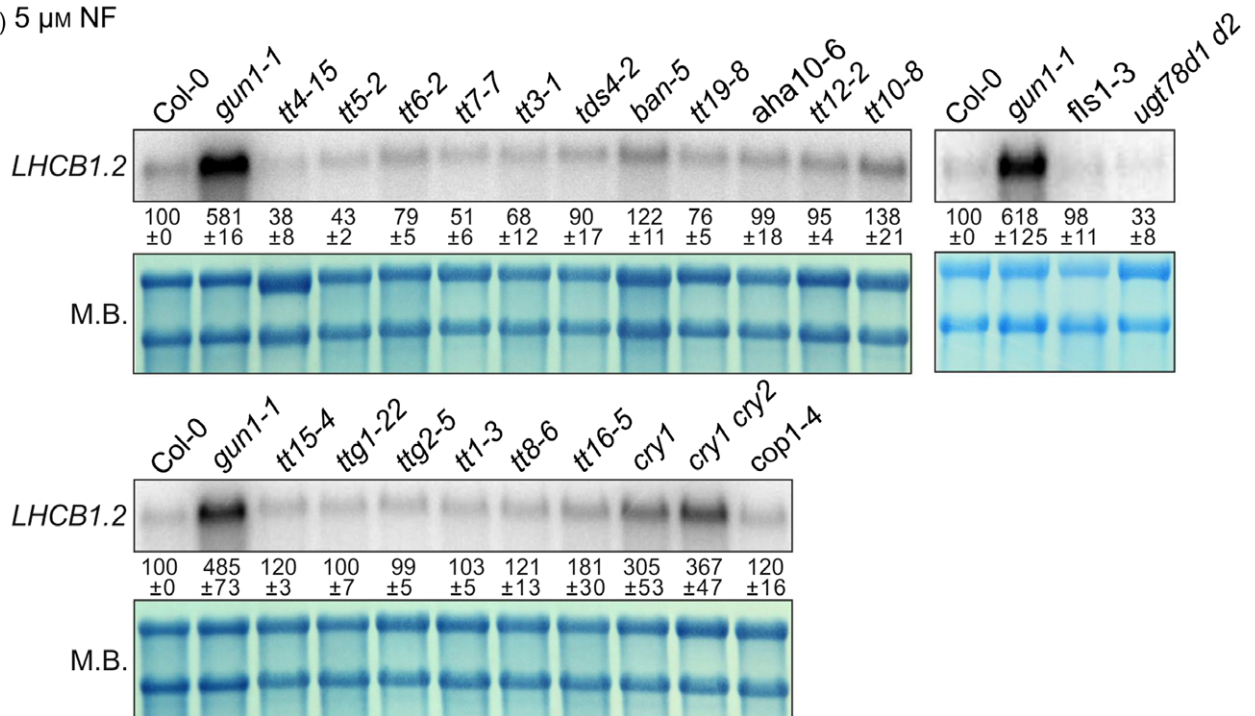


Figure 6. Analysis of *LHCb1.2* transcript levels of the wild type (WT), *gun1*, *cry1*, *cry1 cry2*, *cop1-4* and mutants associated with phenylpropanoid biosynthesis grown in the presence of inhibitors. WT and the mutants described in the legend to Figure 6 were grown for 5 days under continuous light (100 µmol photons m⁻² sec⁻¹) on MS plates supplemented with (a) 50 µg ml⁻¹ lincomycin (LIN) or (b) 5 µM norflurazon (NF). *LHCb1.2* mRNA levels were determined by Northern blot analyses. The methylene blue-stained blots served as loading controls (M.B.).

conditions in *holi6/irx3* and *irx1* seedlings (Figure S5b), implying that the higher temperature overrides the capability of secondary cell wall mutants to green on LIN. Moreover,

the potential greening capacity of *rsw1-1* seedlings on LIN might be masked by the temperature sensitivity of this mutant.

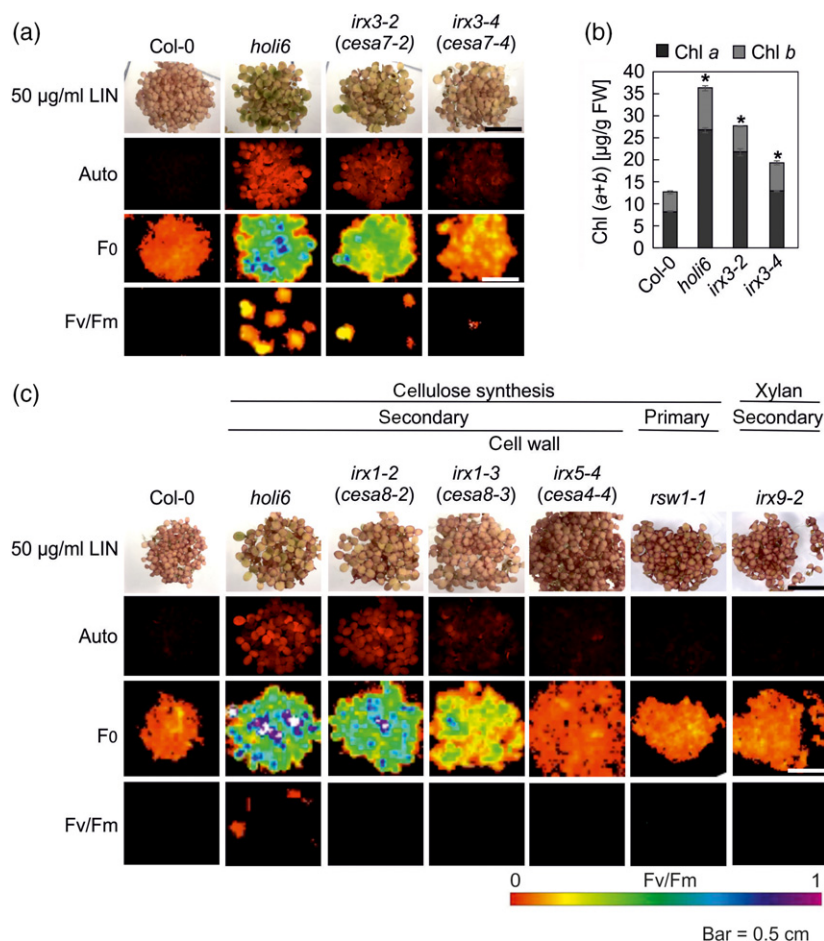


Figure 7. Phenotypes of the wild type (WT), *holi6* and mutants associated with cell-wall synthesis grown on low lincomycin (LIN). (a) WT, *holi6*, *irx3-2* and *irx3-4* mutants were grown for 5 days under continuous light ($100 \mu\text{mol photons m}^{-2} \text{sec}^{-1}$) on MS plates supplemented with low LIN ($50 \mu\text{g ml}^{-1}$). Autofluorescence after UV excitation was monitored. The red fluorescence served as an indicator for chlorophyll accumulation. The maximum quantum yield of photosystem II (F_v/F_m) was measured with an imaging Chl fluorometer (Imaging PAM). (b) Determination of the total chlorophyll (Chl a + b) content of 5-day-old seedlings. Pigments were acetone-extracted, measured spectrophotometrically and concentrations were determined as described by Porra et al. (1989). Data are shown as mean values \pm SDs from three biological replicates. Each replicate pool contained more than 20 seedlings. Significant differences were identified by Tukey's test ($P < 0.05$). (c) WT, *holi6*, *irx1-2*, *irx1-3*, *irx5-4*, *irx9-2* and *rsw1-1* mutants were grown for 5 days under continuous light ($100 \mu\text{mol photons m}^{-2} \text{sec}^{-1}$) on MS plates supplemented with low LIN ($50 \mu\text{g ml}^{-1}$). Autofluorescence after UV excitation was monitored. The red fluorescence served as an indicator for chlorophyll accumulation. The initial Chl a fluorescence (F_0) and the maximum quantum yield of photosystem II (F_v/F_m) were measured with an imaging Chl fluorometer (Imaging PAM).

In sum, it can be concluded that cellulose defects specifically in the secondary cell wall promote seedling greening, and that deactivation of IRX3 results in the strongest greening phenotype.

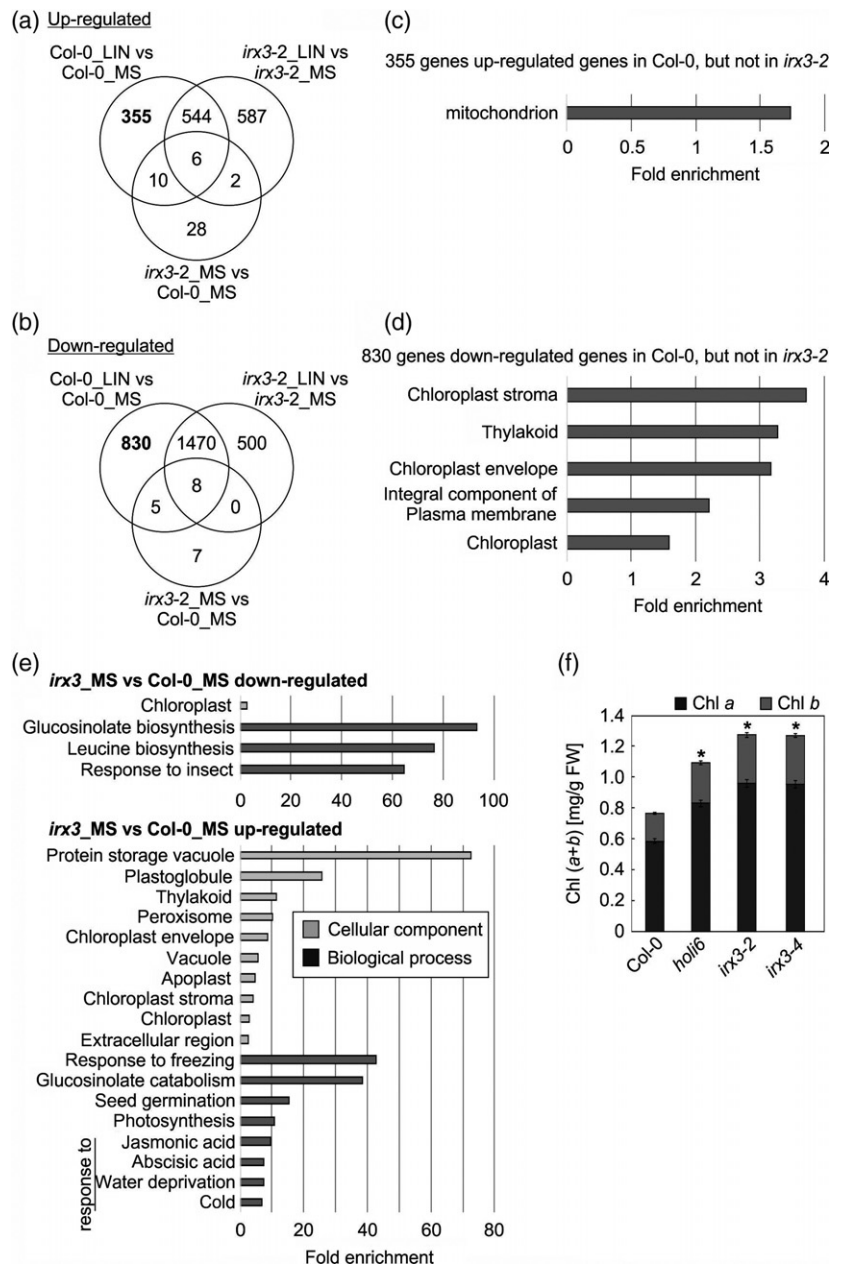
The *irx3* mutant behaves like a *gun* mutant on low LIN

A defect in IRX1 or IRX5, both of which are specific for the secondary cell wall CESA complex, results in the upregulation of ABA-responsive genes (Hernandez-Blanco *et al.*, 2007). Moreover, *LHCB1.2* mRNA expression is higher when the *holi6* mutant is grown on low LIN, as well as in control conditions (Figure 3). To investigate the behavior of ABA-responsive genes and nuclear genes for chloroplast proteins on a transcriptome-wide level in *irx3* mutants, RNA-Seq analysis was performed on RNA isolated from 5-day-old WT and *irx3-2* seedlings grown in the absence of LIN (control) or on low LIN. Low LIN elicited substantial (more than twofold) changes in gene expression in the WT (915 up; 2313 down) and *irx3-2* (1139 up; 1978 down) seedlings (Figure 8a,b; Table S2). Of the genes up- and down-regulated in WT seedlings upon LIN treatment, 39 and 36%, respectively, were dependent on the presence of functional IRX3, namely those that were not more than

twofold differentially expressed in *irx3-2*. Gene ontology (GO) analysis (Huang *et al.*, 2009) of these IRX3-dependent genes identified an enrichment for the cellular component category 'mitochondria' among the 39% upregulated genes (Figure 8c), and in the categories 'chloroplast stroma', 'thylakoid', 'chloroplast envelope', 'integral component of plasma membrane' and 'chloroplast' among the 36% downregulated genes (Figure 8d). This showed that, in addition to *LHCB1.2*, other photosynthesis-related genes were de-repressed in *irx3* seedlings.

When grown under control conditions (without LIN), the transcriptome of the *irx3-2* mutant showed only moderate changes relative to the WT: the mRNA levels of 20 (41) or 46 (70) genes were significantly reduced or elevated (by more than 2.0- and 1.5-fold, respectively) (Figure 8a,b; Table S2). Analyses of the 1.5-fold changes revealed that in the downregulated gene set, only 'chloroplast' was significantly enriched in the cellular component category (CC), whereas the biological process (BP) categories 'glucosinolate biosynthesis', 'leucine biosynthesis' and 'response to insect' were more than 60-fold enriched (Figure 8e). In the upregulated gene set, the CC category 'protein storage vacuole' and several chloroplast-associated categories like

Figure 8. RNA-Seq analysis of 5-day-old WT and *irx3-2* seedlings. Seedlings were grown for 5 days on MS or on MS plates supplemented with $50 \mu\text{g ml}^{-1}$ LIN (LIN). Venn diagrams depict the degree of overlap between the sets of genes whose expression levels were down- (a) or up-regulated (b) by at least twofold in the indicated comparisons. Gene ontology (GO) analysis of genes whose expression was down- (c) or upregulated (d) in the indicated comparisons. GO annotations for the cellular component category were extracted from DAVID (Huang da *et al.*, 2009). GO terms for genes with a >1.5 -fold change and a Benjamini corrected value of <0.05 are shown. (e) Gene ontology (GO) analysis of genes whose expression was down- or upregulated in *irx3* seedlings grown on MS (without LIN) compared to WT. GO annotations for the cellular component and biological process categories were extracted from DAVID (Huang da *et al.*, 2009). GO terms with a Benjamini corrected value of <0.05 are shown. (f) Determination of the total chlorophyll (Chl *a* + *b*) content of 5-day-old seedlings. Pigments were acetone-extracted, measured spectrophotometrically, and concentrations were determined as described (Porra *et al.*, 1989). Data are shown as mean values \pm SD from three biological replicates. Each replicate pool contained more than 20 seedlings. Significant differences were identified by Tukey's test ($P < 0.05$).



'plastoglobule', 'thylakoid', 'envelope' and 'stroma' were enriched, and in the BP category 'response to freezing' and 'glucosinolate catabolism' were enriched approximately 40-fold, and 'seed germination', 'photosynthesis', 'response to jasmonic acid' and 'response to abscisic acid' were enriched approximately 10-fold, respectively (Figure 8e; Table 1). Among the abscisic acid (ABA)-responsive genes were the genes for the chloroplast-localized proteins COLD-REGULATED 15a (COR15a) and COR15b. Of note is also the slight (approximately 1.4-fold) but significant induction of genes encoding several Lhcb proteins and subunits of photosystems I and II (Figure 3; Tables S2 and S3), which was reflected in an approximately 1.5-fold

higher chlorophyll content in 5-day-old *holi6* and *irx3* mutant seedlings (Figure 8f).

Taken together, these results suggest a role for the secondary cell wall in seedling greening, even under normal growth conditions. Moreover, a defect in IRX3 results in a weak *gun* phenotype on low LIN and leads to altered ABA metabolism or sensitivity.

DISCUSSION

Norflurazon is an inhibitor of phytoene desaturase and blocks carotenoid biosynthesis, whereas LIN binds to the 50S subunit of the plastid ribosome, thus inhibiting protein synthesis in the organelle. Treatment of seedling plants

Table 1 Differential expression of ABA-responsive genes, and genes involved in chloroplast biogenesis and light reactions in 5-day-old *irx3-2* mutant seedlings, compared with Col-0

Locus identifier	Fold change	Description	Gene symbol
Chloroplast			
AT2G20570	1.47	GOLDEN2-LIKE 1	GLK1
AT1G61520	1.33	PSI CHLOROPHYLL A/B BINDING PROTEIN 3	LHCA3
AT3G47470	1.39	PSI CHLOROPHYLL A/B BINDING PROTEIN A4	LHCA4
AT1G29910	1.36	PSII CHLOROPHYLL A/B BINDING PROTEIN 3	LHCB1.2
AT2G34430	1.41	PSII CHLOROPHYLL A/B BINDING PROTEIN B1	LHCB1.4
AT2G05100	1.51	PSII CHLOROPHYLL A/B BINDING PROTEIN 2.1	LHCB2.1
AT2G05070	1.63	PSII CHLOROPHYLL A/B BINDING PROTEIN 2.2	LHCB2.2
AT3G27690	1.53	PSII CHLOROPHYLL A/B BINDING PROTEIN 2.3	LHCB2.3
AT5G54270	1.47	PSII CHLOROPHYLL A/B BINDING PROTEIN 3	LHCB3.1
AT4G10340	1.33	PSII CHLOROPHYLL A/B BINDING PROTEIN 5	LHCB5
AT4G27440	1.32	PROTOCHLOROPHYLLIDE OXIDOREDUCTASE B	PORB
AT4G28750	1.46	PSI SUBUNIT E-1	PSAE-1
AT1G52230	1.40	PSI SUBUNIT H2	PSAH2
AT1G08380	1.40	PSI SUBUNIT O	PSAO
ATCG00220	1.40	PSII SUBUNIT M	PSBM
AT4G05180	1.36	PSII SUBUNIT Q-2	PSBQ-2
AT2G30570	1.33	PSII SUBUNIT W	PSBW
AT1G67740	1.35	PSII SUBUNIT Y	PSBY
ABA-responsive			
AT2G42540	3.44	COLD-REGULATED 15A	COR15A
AT2G42530	3.17	COLD REGULATED 15B	COR15B
AT1G29395	2.83	COLD REGULATED 314 INNER MEMBRANE 1	COR413IM1
AT5G15970	1.98	Stress-induced protein KIN2/COLD-REGULATED 6.6	KIN2
AT1G52400	2.19	BETA GLUCOSIDASE 18	BGLU18
AT4G04020	1.61	FIBRILLIN	FBN1A
AT4G23600	2.74	CORONATINE INDUCED 1	CORI3
AT4G28520	4.52	CRUCIFERIN 3	CRU3
AT5G25980	3.52	GLUCOSIDE GLUCOHYDROLASE 2	TGG2
AT5G44120	4.67	CRUCIFERINA	CRA1

Seedlings were grown on MS without supplementation of LIN. Differential expression was determined with RNA-Seq analysis (Tables S2 and S3) and fold changes are represented. PS, photosystem.

with NF or LIN prevents greening, promotes anthocyanin accumulation and suppresses the light-induced transcription of nuclear genes for photosynthesis, such as *LHCB1.2*. In all known *gun* mutants, *LHCB1.2* expression is partly de-repressed in the presence of NF, but only a subset of *gun* mutants display this phenotype in the presence of LIN

(Koussevitzky *et al.*, 2007; Ruckle *et al.*, 2007). We attempted to isolate further mutants that can better cope with LIN. High concentrations of LIN (220 $\mu\text{g ml}^{-1}$) were used in previous studies (Koussevitzky *et al.*, 2007; Ruckle *et al.*, 2007; Choy *et al.*, 2008; Cottage *et al.*, 2010; Sun *et al.*, 2016), and we found that a greater than fourfold lower concentration (50 $\mu\text{g ml}^{-1}$) of LIN still repressed nucleus-encoded photosynthesis genes (Figure 1b). Moreover, the use of low LIN uncovered a clear phenotypical difference between *gun1-1* and WT seedlings, as cotyledons were larger and anthocyanin accumulation was less pronounced in the *gun1-1* mutant (Figure 1a). With the exception of the *hon* mutant screen, in which lower NF and light dosages were used (Saini *et al.*, 2011), all previous *gun* mutant screens used reporter genes to identify mutants with de-repressed *LHCB* expression (Kleine and Leister, 2016). In contrast, we attempted to isolate mutants based on visually discernible differences from the WT when grown on low LIN. Although the earlier *hon* mutant screen identified mutants that are affected in chloroplast protein homeostasis, our low-LIN screen led to the identification of '*holi*' and additional '*hon*' mutants for proteins involved in: (i) the flavonoid pathway; and (ii) secondary cell wall formation (Figure 4).

We used 5-day-old seedlings grown on MS supplemented with sucrose to investigate phenylpropanoid accumulation and parameters associated with chloroplast development, i.e. the maximum quantum yield of photosystem II, *LHCB1.2* expression levels and greening. In 1992, it was found that several transcripts for enzymes of the flavonoid biosynthetic pathway reached a maximum in 3-day-old *Arabidopsis* seedlings grown in continuous light. The authors concluded that the peak anthocyanin content appeared to coincide with the maturation of chloroplasts, and the associated switch to photoautotrophic growth (Kubasek *et al.*, 1992). Subsequent work showed that, in the presence of 2% sucrose, and in the absence of inhibitors, anthocyanin accumulation reaches a maximum in 5-day-old seedlings (Cottage *et al.*, 2010). In addition to the presence of disaccharides, the induction of anthocyanins depends on a functional photosynthetic electron transport chain and on light (Jeong *et al.*, 2010). Thus, the light-signaling mutants *cry1* and *hy5* exhibit significant inhibition of anthocyanin accumulation (Ahmad *et al.*, 1995; Jeong *et al.*, 2010). Notably, *cry1* and *hy5* mutants have been identified as *gun* mutants (Ruckle *et al.*, 2007), and lower levels of anthocyanins were noted in the original set (*gun1–gun5*) in this present study and in other studies (Cottage *et al.*, 2010; Voigt *et al.*, 2010). The idea that changes in anthocyanin accumulation might trigger de-repression of *LHCB1.2* in *gun* mutants has previously been rejected (Voigt *et al.*, 2010); however, the consistent observation of lowered anthocyanin accumulation in mutants showing the *gun* phenotype prompted us to re-evaluate

this putative link. Because anthocyanins represent the only visibly perceptible products of the phenylpropanoid pathway, we performed reverse-phase UPLC to profile the accumulation of phenylpropanoids that absorb in the UV region (280 nm) of the spectrum (Figure S3; Table S1) and found that the kaempferol derivative k3 is less abundant in *gun* mutants after inhibitor treatment. A second approach using various mutants blocked at different steps in the phenylpropanoid pathway (Figures 6 and 7) strongly suggests that neither the abundance of k3 nor that of any other intermediate of the phenylpropanoid pathway is correlated with *LHCB1.2* expression, however. Therefore, our data suggest that changes in phenylpropanoid levels cannot account for *LHCB1.2* de-repression in inhibitor-treated *gun* mutants.

Of all the mutants identified here, *holi6* displayed the strongest chlorophyll autofluorescence when grown in the presence of low LIN (Figures 2 and 8). *HOLI6* encodes the cellulose synthase subunit CESA7, also named IRX3, because in *irx* mutants the xylem collapses (Brown *et al.*, 2005). Further results indicated that perturbation of cellulose formation specifically in the secondary cell wall leads to a happy-on-lincomycin phenotype (Figure 7). This may seem counterintuitive, but the weakening of the cell wall caused by defects in IRX1, IRX3 or IRX5 also confers enhanced resistance to some pathogens (Hernandez-Blanco *et al.*, 2007; Miedes *et al.*, 2014). In analogy to our findings that the *rsw1-1* mutant with a defect in the primary cell wall is not able to green on LIN (Figure 7), susceptibility to these pathogens was not altered in mutants that affect the primary cell wall, like the *cesa3* and *rsw1* mutants (Hernandez-Blanco *et al.*, 2007), although *cesa3* mutants can be more resistant to other pathogens (Ellis *et al.*, 2002). Could this mean that a weakened secondary cell wall might confer resistance to lincomycin? Presumably not, because the chlorophyll content of *irx3* mutants is already higher than that of the WT under normal growth conditions (Figure 8). Moreover, the disease resistance phenotype of *irx1*, *irx3* and *irx5* mutants has been attributed in part to the constitutive activation of plant immune responses rather than to alterations in the passive wall barrier. In *irx1-6* and *irx5-5* plants a large number of ABA-regulated genes are constitutively upregulated (Hernandez-Blanco *et al.*, 2007), which is in agreement with an increased accumulation of ABA in the *irx1-6* mutant (Chen *et al.*, 2005). Accordingly, we found that, in the *irx3-2* mutant, ABA-responsive genes are upregulated under normal growth conditions (Figure 8). ABA has previously been shown to have an impact on *LHCB1.2*, plastid-encoded gene expression (Koussevitzky *et al.*, 2007; Voigt *et al.*, 2010; Yamburenko *et al.*, 2013) and plastid differentiation (Rohde *et al.*, 2000; Penfield *et al.*, 2006; Kim *et al.*, 2009). ABA seems to affect plastid differentiation in opposing ways. High concentrations suppress the expression of certain nucleus-encoded chloroplast proteins as well as plastid formation in etiolated and light-grown seedlings, and in

seedlings grown in the presence of NF (Penfield *et al.*, 2006; Koussevitzky *et al.*, 2007), whereas lower concentrations stimulate these processes (Voigt *et al.*, 2010; Kim *et al.*, 2012). The tetrapyrrole biosynthesis proteins GUN4 and GUN5 (Voigt *et al.*, 2010), the PPR protein GUN1 (Cottage *et al.*, 2010) and GREENING AFTER EXTENDED DARKNESS 1 (GED1) (Choy *et al.*, 2008) all enhance seedling development in the presence of ABA. Interestingly, the *ged1* mutant was identified in a further attempt to isolate *gun1*-like mutants (Gray *et al.*, 2003; Choy *et al.*, 2008); however, like *holi6*, *ged1* is not a true *gun* mutant, because *RBCS* and *LHCB1* mRNA levels are already elevated in the absence of inhibitors, and *ged1* shows only a very subtle *gun* phenotype upon treatment with NF or LIN (Choy *et al.*, 2008).

The phenomenon of signaling from an altered cell wall to influence seedling photomorphogenesis in the dark has been recognized in the case of sugar- (Li *et al.*, 2007) and zinc-responsive (Sinclair *et al.*, 2017) growth and development. Our results suggest that defects in secondary cell walls also generate signals that modify nuclear gene expression and promote seedling greening, possibly via altered ABA metabolism or sensing.

EXPERIMENTAL PROCEDURES

Plant material and growth conditions

The mutant lines used in this study are listed in Table S4. The *irx3-2* mutant was genotyped with the following primers: SAIL_885_D10_LP, 5'-AAGTTGGATCATGCAAGATG-3'; SAIL_885_D10_RP, 5'-CCAGCTGCAATTCGAGATAC-3', and LB, 5'-ATTTT GCCGATTCGGAAC-3'. Surface-sterilized seeds were sown on Murashige and Skoog plates containing 0.8% (w/v) agar (pH 5.8), and stratified for at least 2 days at 4°C. The growth medium contained 1% (w/v) sucrose, unless indicated otherwise. Seedlings were grown at 22°C under continuous illumination (100 $\mu\text{mol photons m}^{-2} \text{sec}^{-1}$) provided by white fluorescent lamps or at 31°C under continuous illumination (80 $\mu\text{mol photons m}^{-2} \text{sec}^{-1}$) provided by LEDs, which corresponds to 100 $\mu\text{mol photons m}^{-2} \text{sec}^{-1}$ provided by white fluorescent lamps). For inhibitor experiments, MS medium was supplemented with the indicated concentration of lincomycin (Sigma-Aldrich, <https://www.sigmaaldrich.com/united-kingdom.html>) or norflurazon (Sigma-Aldrich).

EMS mutagenesis and whole-genome resequencing

Col-0 seeds were mutagenized using 0.2% (v/v) EMS (Sigma-Aldrich). The mutagenized M₁ plants were grown in pools of 500 to produce the M₂ generation of seeds. M₂ plants were screened for *holi* or *hon* phenotypes. Segregating F₂ populations were generated by backcrossing *holi* or *hon* mutants with the parental Col-0 line. To identify the causative mutations, positive pools of 50 plants each were selected based on their *holi* or *hon* mutant phenotype. DNA was extracted with the DNeasy Plant Mini kit (QIAGEN, <https://www.qiagen.com>). Preparation of 350-bp insert DNA libraries and 150-bp paired-end sequencing was carried out at Novogene Biotech (<https://en.novogene.com>) on an Illumina HiSeq 2500 system (Illumina, <https://www.illumina.com>) with standard Illumina protocols. The sequencing depth was at least 7 G of raw data per sample, which corresponds to a more than 50-fold

coverage of the *A. thaliana* genome. After grooming FASTQ files, adaptors were removed with TRIMMOMATIC (Bolger *et al.*, 2014), reads were mapped with BWA (Li and Durbin, 2009), with parameters 'mem -t 4 -k 32 -M' to the TAIR10 annotation, and duplicates were removed by SAMTOOLS (Li *et al.*, 2009) with the RMDUP tool. Single-nucleotide polymorphisms (SNPs) were identified using SAMTOOLS (Li *et al.*, 2009) with the parameter 'mpileup -m 2 -F 0.002 -d 1000'. Only SNPs that were supported by more than four reads with a mapping quality of > 20 were retained. To identify the SNPs specific for the *holi* and *hon* mutants, the SNPs between each of the *holi* and *hon* mutants were compared with the SNPs of our Col-0 strain. The resulting *holi*- and *hon*-specific SNP lists were subjected to the web application CandiSNP (Etherington *et al.*, 2014), which generates SNP density plots. The output list of CandiSNP was screened for non-synonymous amino acid changes and for the G/C@A/T transitions that were likely to be caused by EMS, with a special focus on the chromosome with the highest SNP density with an allele frequency of > 0.75.

Detection of chlorophyll autofluorescence

Chlorophyll autofluorescence of cotyledons was recorded with a Lumar V12 microscope equipped with the filter set Lumar 09 (no. 485009) connected to an AxioCam digital camera (Zeiss, <https://www.zeiss.com>).

Chlorophyll fluorescence measurements

Chlorophyll fluorescence was detected using an imaging Chl fluorometer (Imaging PAM, M-Series; Walz, <https://www.walz.com>) equipped with the computer-operated PAM control unit IMAGE-MAXI, as described previously (Xu *et al.*, 2019).

Chlorophyll concentration measurements

For chlorophyll extraction, the cotyledons were blotted with filter paper to remove excess water, and hypocotyls were removed to ensure that only chlorophyll from the cotyledons was extracted. Briefly, 50-mg (fresh weight) cotyledon samples were ground and chlorophyll was extracted by adding 4 ml of 80% (v/v) acetone to each sample. The extract was centrifuged at 17 900 *g* for 10 min and the pigments were quantified as described previously (Porra *et al.*, 1989).

Determination of phenylpropanoid levels

Extraction, detection and analysis of phenylpropanoid contents was done as described in Appendix S1.

cDNA synthesis and quantitative RT-PCR analysis

Total RNA was extracted with the RNeasy Plant Mini kit (QIAGEN) according to the manufacturer's protocol, and 2 µg of the RNA was employed to synthesize cDNA using the iScript cDNA Synthesis Kit (Bio-Rad, <https://www.bio-rad.com>). RT-qPCR analysis was performed on a Bio-Rad iQ5 real-time PCR instrument with the iQ SYBR Green Supermix (Bio-Rad). Each sample was quantified in triplicate and normalized using AT4G36800, which codes for a RUB1 conjugating enzyme (*RCE1*), as an internal control. The following primers were used: RCE1-RT-F, 5'-CTGTTACCGAACCAATTC-3; RCE1-RT-R, 5-GGAAAAAGGTCTGACCGACA-3; LHCB1.2-RT-F, 5-CCGTGAGCTAGAAGTTATCC-3; LHCB1.2-RT-R, 5-GTTTC CCAAGTAATCGAGTCC-3; CA1-RT-F, 5-GAGAAATACGAAACCAACCT-3; CA1-RT-R, 5-ACATAAGCCCTTTGATCCCA-3; IRX3-exon1-2-RT-F, 5-AACCATGAAGAGCCAAAGCC-3; IRX3-exon1-2-RT-R, 5-TCGTACTCATAGCAAGGTCTACAC-3; IRX3-exon11-12-RT-F, 5-ATC

ATGCCACCGATAAGCAC-3; and IRX3-exon11-12-RT-R, 5-GAGGGA TCAGCAGTGTGTC-3.

RNA gel-blot analysis

Total RNA was purified using the TRIzol reagent (Invitrogen, now ThermoFisher Scientific, <https://www.thermofisher.com>). To eliminate contaminating genomic DNA, RNA was treated with DNase I (New England BioLabs, <https://www.neb.com>). Total RNA (5 µg) was fractionated on a denaturing agarose gel, blotted onto a nylon membrane (Hybond-XL; GE Healthcare, <https://www.gehealthcare.com>) and subsequently cross-linked by UV light. Hybridizations were performed at 65°C according to standard protocols. Details of these probes have been described previously (Kacprzak *et al.*, 2019).

RNA sequencing (RNA-Seq) and data analysis

Total RNA from plants was isolated using Trizol (Invitrogen, now ThermoFisher Scientific) and purified using Direct-zol™ RNA MiniPrep Plus columns (Zymo Research, <https://www.zymoresearch.com>) according to the manufacturer's instructions. RNA integrity and quality were assessed with an Agilent 2100 Bioanalyzer (Agilent, <https://www.agilent.com>). Ribosomal RNA depletion, the generation of RNA-Seq libraries and 150-bp paired-end sequencing on an Illumina HiSeq 2500 system (Illumina) were conducted at Novogene Biotech with standard Illumina protocols. Three independent biological replicates were used per genotype.

RNA-Seq reads were analyzed on the Galaxy platform (Afgan *et al.*, 2016), as described by Xu *et al.* (2019). Sequencing data have been deposited in the National Center for Biotechnology Information (NCBI) Gene Expression Omnibus (GEO) (Edgar *et al.*, 2002) and are accessible through the GEO series accession number GSE130337.

Data analysis and statistical tests

One-way analysis of variance (ANOVA) was performed to determine statistical significances between genotypes ($P < 0.05$), followed by Tukey's test for differences of group means at a 95% confidence interval using SPSS STATISTICS 17.0.

ACKNOWLEDGEMENTS

We thank Bernd Weisshaar and Anton Schäffner for providing seeds of the phenylpropanoid biosynthesis mutants. We thank Paul Hardy and Bernd Weisshaar for their critical reading of the article and Elisabeth Gerick for excellent technical assistance.

CONFLICT OF INTEREST

The authors declare no competing or financial interests.

AUTHOR CONTRIBUTIONS

Conceptualization: TK, DX Experiments: DX, RD, AG, H-PM, and TK Writing original draft: TK Writing review and editing: DL, DX, RD, AG, H-PM, and TK Supervision: TK Funding acquisition: TK and DL.

FUNDING

This work was supported by the Deutsche Forschungsgemeinschaft (KL 2362/1-1 and TRR175, project C01, to T.K.;

TRR175, project C05, to D.L.). D.X. was supported by the China Scholarship Council fellowship.

DATA AVAILABILITY STATEMENT

RNA sequencing data have been deposited in the NCBI GEO (Edgar *et al.*, 2002) and are accessible through the GEO series accession number GSE130337.

SUPPORTING INFORMATION

Additional Supporting Information may be found in the online version of this article.

Figure S1. Illustration of the phenylpropanoid and flavonoid pathways in Arabidopsis.

Figure S2. Phenotypes of *gun* mutants grown in the presence of lincomycin (LIN) or norflurazon (NF).

Figure S3. Determination of phenylpropanoid contents of 5-day-old WT and *gun* mutant seedlings.

Figure S4. Confirmation of the *irx3-2* T-DNA insertion mutant.

Figure S5. Phenotypes of WT, *holi6* and mutants associated with cell-wall synthesis grown at 31°C on MS without or with low lincomycin (LIN).

Table S1. Detection of major phenylpropanoids in methanolic extracts from 5-day-old seedlings grown on MS plates without supplementation or supplemented with either 5 µM NF or 220 µg ml⁻¹ LIN.

Table S2. Genes with transcript levels that differed significantly from Col-0 in 5-day-old *irx3-2* seedlings grown on MS plates without supplementation or supplemented with 50 µg ml⁻¹ LIN.

Table S3. Genes with transcript levels that differed significantly from Col-0 in 5-day-old *irx3-2* seedlings grown on MS plates were sorted into different categories.

Table S4. *Arabidopsis thaliana* mutants used in this study.

Appendix S1. Supplemental materials and methods.

REFERENCES

- Afgan, E., Baker, D., van den Beek, M. *et al.* (2016) The Galaxy platform for accessible, reproducible and collaborative biomedical analyses: 2016 update. *Nucleic Acids Res.* **44**, W3–W10.
- Ahmad, M., Lin, C. and Cashmore, A.R. (1995) Mutations throughout an Arabidopsis blue-light photoreceptor impair blue-light-responsive anthocyanin accumulation and inhibition of hypocotyl elongation. *Plant J.* **8**, 653–658.
- Appelhaagen, I., Thiedig, K., Nordholt, N., Schmidt, N., Huep, G., Sagasser, M. and Weisshaar, B. (2014) Update on transparent testa mutants from Arabidopsis thaliana: characterisation of new alleles from an isogenic collection. *Planta*, **240**, 955–970.
- Arioli, T., Peng, L., Betzner, A.S. *et al.* (1998) Molecular analysis of cellulose biosynthesis in Arabidopsis. *Science*, **279**, 717–720.
- Bauer, S., Vasu, P., Persson, S., Mort, A.J. and Somerville, C.R. (2006) Development and application of a suite of polysaccharide-degrading enzymes for analyzing plant cell walls. *Proc. Natl Acad. Sci. USA*, **103**, 11417–11422.
- Bolger, A.M., Lohse, M. and Usadel, B. (2014) Trimmomatic: a flexible trimmer for Illumina sequence data. *Bioinformatics*, **30**, 2114–2120.
- Bonawitz, N.D., Soltan, W.L., Blatchley, M.R., Powers, B.L., Hurlock, A.K., Seals, L.A., Weng, J.K., Stout, J. and Chapple, C. (2012) REF4 and RFR1, subunits of the transcriptional coregulatory complex mediator, are required for phenylpropanoid homeostasis in Arabidopsis. *J. Biol. Chem.* **287**, 5434–5445.
- Brown, D.M., Zeef, L.A., Ellis, J., Goodacre, R. and Turner, S.R. (2005) Identification of novel genes in Arabidopsis involved in secondary cell wall formation using expression profiling and reverse genetics. *Plant Cell*, **17**, 2281–2295.

- Chan, K.X., Phua, S.Y., Crisp, P., McQuinn, R. and Pogson, B.J. (2016) Learning the languages of the chloroplast: retrograde signaling and beyond. *Annu. Rev. Plant Biol.* **67**, 25–53.
- Chen, Z., Hong, X., Zhang, H., Wang, Y., Li, X., Zhu, J.K. and Gong, Z. (2005) Disruption of the cellulose synthase gene, *AtCesA8/IRX1*, enhances drought and osmotic stress tolerance in Arabidopsis. *Plant J.* **43**, 273–283.
- Chi, W., Sun, X. and Zhang, L. (2013) Intracellular signaling from plastid to nucleus. *Annu. Rev. Plant Biol.* **64**, 559–582.
- Choy, M.K., Sullivan, J.A., Theobald, J.C., Davies, W.J. and Gray, J.C. (2008) An Arabidopsis mutant able to green after extended dark periods shows decreased transcripts of seed protein genes and altered sensitivity to abscisic acid. *J. Exp. Bot.* **59**, 3869–3884.
- Cottage, A., Mott, E.K., Kempster, J.A. and Gray, J.C. (2010) The Arabidopsis plastid-signalling mutant *gun1* (genomes uncoupled1) shows altered sensitivity to sucrose and abscisic acid and alterations in early seedling development. *J. Exp. Bot.* **61**, 3773–3786.
- Edgar, R., Domrachev, M. and Lash, A.E. (2002) Gene expression omnibus: NCBI gene expression and hybridization array data repository. *Nucleic Acids Res.* **30**, 207–210.
- Ellis, C., Karafyllidis, I., Wasternack, C. and Turner, J.G. (2002) The Arabidopsis mutant *cev1* links cell wall signaling to jasmonate and ethylene responses. *Plant Cell*, **14**, 1557–1566.
- Etherington, G.J., Monaghan, J., Zipfel, C. and MacLean, D. (2014) Mapping mutations in plant genomes with the user-friendly web application CandiSNP. *Plant Methods*, **10**, 41.
- Gray, J.C., Sullivan, J.A., Wang, J.H., Jerome, C.A. and MacLean, D. (2003) Coordination of plastid and nuclear gene expression. *Philos. Trans. R. Soc. Lond. B Biol. Sci.*, **358**, 135–145; discussion 144–135.
- Hernandez-Blanco, C., Feng, D.X., Hu, J. *et al.* (2007) Impairment of cellulose synthases required for Arabidopsis secondary cell wall formation enhances disease resistance. *Plant Cell*, **19**, 890–903.
- Huang, D.W., Sherman, B.T. and Lempicki, R.A. (2009) Systematic and integrative analysis of large gene lists using DAVID Bioinformatics Resources. *Nature Protoc.* **4**, 44–57.
- Jeong, S.W., Das, P.K., Jeoung, S.C. *et al.* (2010) Ethylene suppression of sugar-induced anthocyanin pigmentation in Arabidopsis. *Plant Physiol.* **154**, 1514–1531.
- Kacprzak, S.M., Mochizuki, N., Naranjo, B., Xu, D., Leister, D., Kleine, T., Okamoto, H. and Terry, M.J. (2019) Plastid-to-nucleus retrograde signalling during chloroplast biogenesis does not require ABI4. *Plant Physiol.* **179**, 18–23.
- Kim, C., Lee, K.P., Baruah, A., Nater, M., Gobel, C., Feussner, I. and Apel, K. (2009) (1)O₂-mediated retrograde signaling during late embryogenesis predetermines plastid differentiation in seedlings by recruiting abscisic acid. *Proc. Natl Acad. Sci. USA*, **106**, 9920–9924.
- Kim, M., Lee, U., Small, I., des Francs-Small, C.C. and Vierling, E. (2012) Mutations in an Arabidopsis mitochondrial transcription termination factor-related protein enhance thermotolerance in the absence of the major molecular chaperone HSP101. *Plant Cell*, **24**, 3349–3365.
- Kleine, T. and Leister, D. (2016) Retrograde signaling: organelles go networking. *Biochim. Biophys. Acta*, **1857**, 1313–1325.
- Kleine, T., Voigt, C. and Leister, D. (2009) Plastid signalling to the nucleus: messengers still lost in the mists? *Trends Genet.* **25**, 185–192.
- Koussevitzky, S., Nott, A., Mockler, T.C., Hong, F., Sabetto-Martins, G., Surpin, M., Lim, J., Mittler, R. and Chory, J. (2007) Signals from chloroplasts converge to regulate nuclear gene expression. *Science*, **316**, 715–719.
- Kubasek, W.L., Shirley, B.W., McKillop, A., Goodman, H.M., Briggs, W. and Ausubel, F.M. (1992) Regulation of flavonoid biosynthetic genes in germinating Arabidopsis seedlings. *Plant Cell*, **4**, 1229–1236.
- Larkin, R.M., Alonso, J.M., Ecker, J.R. and Chory, J. (2003) GUN4, a regulator of chlorophyll synthesis and intracellular signaling. *Science*, **299**, 902–906.
- Leister, D. and Kleine, T. (2016) Definition of a core module for the nuclear retrograde response to altered organellar gene expression identifies GLK overexpressors as *gun* mutants. *Physiol. Plant*, **157**, 297–309.
- Li, H. and Durbin, R. (2009) Fast and accurate short read alignment with Burrows-Wheeler transform. *Bioinformatics*, **25**, 1754–1760.
- Li, Y., Smith, C., Corke, F., Zheng, L., Merali, Z., Ryden, P., Derbyshire, P., Waldron, K. and Bevan, M.W. (2007) Signaling from an altered cell wall to the nucleus mediates sugar-responsive growth and development in Arabidopsis thaliana. *Plant Cell*, **19**, 2500–2515.

- Li, H., Handsaker, B., Wysoker, A., Fennell, T., Ruan, J., Homer, N., Marth, G., Abecasis, G., Durbin, R. and 1000 Genome Project Data Processing Subgroup. (2009) The sequence alignment/map format and SAMtools. *Bioinformatics*, **25**, 2078–2079.
- Liang, M., Davis, E., Gardner, D., Cai, X. and Wu, Y. (2006) Involvement of AtLAC15 in lignin synthesis in seeds and in root elongation of Arabidopsis. *Planta*, **224**, 1185–1196.
- Martin, G., Leivar, P., Ludevid, D., Tepperman, J.M., Quail, P.H. and Monte, E. (2016) Phytochrome and retrograde signalling pathways converge to antagonistically regulate a light-induced transcriptional network. *Nat. Commun.* **7**, 11431.
- Meents, M.J., Watanabe, Y. and Samuels, A.L. (2018) The cell biology of secondary cell wall biosynthesis. *Ann. Bot.* **121**, 1107–1125.
- Miedes, E., Vanholme, R., Boerjan, W. and Molina, A. (2014) The role of the secondary cell wall in plant resistance to pathogens. *Front. Plant Sci.* **5**, 358.
- Mochizuki, N., Brusslan, J.A., Larkin, R., Nagatani, A. and Chory, J. (2001) Arabidopsis genomes uncoupled 5 (GUN5) mutant reveals the involvement of Mg-chelatase H subunit in plastid-to-nucleus signal transduction. *Proc. Natl Acad. Sci. USA*, **98**, 2053–2058.
- Mochizuki, N., Tanaka, R., Tanaka, A., Masuda, T. and Nagatani, A. (2008) The steady-state level of Mg-protoporphyrin IX is not a determinant of plastid-to-nucleus signaling in Arabidopsis. *Proc. Natl Acad. Sci. USA*, **105**, 15184–15189.
- Moulin, M., McCormac, A.C., Terry, M.J. and Smith, A.G. (2008) Tetrapyrrole profiling in Arabidopsis seedlings reveals that retrograde plastid nuclear signaling is not due to Mg-protoporphyrin IX accumulation. *Proc. Natl Acad. Sci. USA*, **105**, 15178–15183.
- Oelmuller, R. and Mohr, H. (1986) Photooxidative destruction of chloroplasts and its consequences for expression of nuclear genes. *Planta*, **167**, 106–113.
- Oelmuller, R., Levitan, I., Bergfeld, R., Rajasekhar, V.K. and Mohr, H. (1986) Expression of nuclear genes as affected by treatments acting on the plastids. *Planta*, **168**, 482–492.
- Penfield, S., Li, Y., Gilday, A.D., Graham, S. and Graham, I.A. (2006) Arabidopsis ABA INSENSITIVE4 regulates lipid mobilization in the embryo and reveals repression of seed germination by the endosperm. *Plant Cell*, **18**, 1887–1899.
- Polko, J. and Kieber, J.J. (2019) The regulation of cellulose biosynthesis in plants. *Plant Cell*, **31**, 282–296.
- Ponce-Toledo, R.I., Deschamps, P., Lopez-Garcia, P., Zivanovic, Y., Benzerara, K. and Moreira, D. (2017) An early-branching freshwater cyanobacterium at the origin of plastids. *Curr. Biol.* **27**, 386–391.
- Porra, R.J., Thompson, W.A. and Kriedemann, P.E. (1989) Determination of accurate extinction coefficients and simultaneous-equations for assaying Chlorophyll-a and Chlorophyll-B extracted with 4 different solvents - verification of the concentration of chlorophyll standards by atomic-absorption spectroscopy. *Biochem. Biophys. Acta*, **975**, 384–394.
- Rohde, A., De Rycke, R., Beeckman, T., Engler, G., Van Montagu, M. and Boerjan, W. (2000) ABI3 affects plastid differentiation in dark-grown Arabidopsis seedlings. *Plant Cell*, **12**, 35–52.
- Ruckle, M.E., DeMarco, S.M. and Larkin, R.M. (2007) Plastid signals remodel light signaling networks and are essential for efficient chloroplast biogenesis in Arabidopsis. *Plant Cell*, **19**, 3944–3960.
- Saini, G., Meskauskiene, R., Pijacka, W., Roszak, P., Sjogren, L.L., Clarke, A.K., Straus, M. and Apel, K. (2011) 'happy on norflurazon' (hon) mutations implicate perturbation of plastid homeostasis with activating stress acclimatization and changing nuclear gene expression in norflurazon-treated seedlings. *Plant J.* **65**, 690–702.
- Sinclair, S.A., Larue, C., Bonk, L. et al. (2017) Etiolated seedling development requires repression of photomorphogenesis by a Small Cell-Wall-Derived Dark Signal. *Curr. Biol.* **27**, 3403–3418.e3407.
- Stern, D.B., Goldschmidt-Clermont, M. and Hanson, M.R. (2010) Chloroplast RNA metabolism. *Annu. Rev. Plant Biol.* **61**, 125–155.
- Stout, J., Romero-Severson, E., Ruegger, M.O. and Chapple, C. (2008) Semidominant mutations in reduced epidermal fluorescence 4 reduce phenylpropanoid content in Arabidopsis. *Genetics*, **178**, 2237–2251.
- Strand, A., Asami, T., Alonso, J., Ecker, J.R. and Chory, J. (2003) Chloroplast to nucleus communication triggered by accumulation of Mg-protoporphyrin IX. *Nature*, **421**, 79–83.
- Sun, X., Xu, D., Liu, Z., Kleine, T. and Leister, D. (2016) Functional relationship between mTERF4 and GUN1 in retrograde signaling. *J. Exp. Bot.* **67**, 3909–3924.
- Susek, R.E., Ausubel, F.M. and Chory, J. (1993) Signal transduction mutants of Arabidopsis uncouple nuclear CAB and RBCS gene expression from chloroplast development. *Cell*, **74**, 787–799.
- Terry, M.J. and Smith, A.G. (2013) A model for tetrapyrrole synthesis as the primary mechanism for plastid-to-nucleus signaling during chloroplast biogenesis. *Front. Plant Sci.* **4**, 14.
- Timmis, J.N., Ayliffe, M.A., Huang, C.Y. and Martin, W. (2004) Endosymbiotic gene transfer: organelle genomes forge eukaryotic chromosomes. *Nat. Rev. Genet.* **5**, 123–135.
- Tohge, T., Nishiyama, Y., Hirai, M.Y. et al. (2005) Functional genomics by integrated analysis of metabolome and transcriptome of Arabidopsis plants over-expressing an MYB transcription factor. *Plant J.* **42**, 218–235.
- Voigt, C., Oster, U., Bornke, F., Jahns, P., Dietz, K.J., Leister, D. and Kleine, T. (2010) In-depth analysis of the distinctive effects of norflurazon implies that tetrapyrrole biosynthesis, organellar gene expression and ABA cooperate in the GUN-type of plastid signalling. *Physiol. Plant*, **138**, 503–519.
- Williamson, R.E., Burn, J.E., Birch, R., Baskin, T.I., Arioli, T., Betzner, A.S. and Cork, A. (2001) Morphology of *rsw1*, a cellulose-deficient mutant of Arabidopsis thaliana. *Protoplasma*, **215**, 116–127.
- Woodson, J.D., Perez-Ruiz, J.M. and Chory, J. (2011) Heme synthesis by plastid ferrochelatase I regulates nuclear gene expression in plants. *Curr. Biol.* **21**, 897–903.
- Xu, D., Marino, G., Klingl, A., Enderle, B., Monte, E., Kurth, J., Hiltbrunner, A., Leister, D. and Kleine, T. (2019) Extrachloroplastic PP7L functions in chloroplast development and abiotic stress tolerance. *Plant Physiol.* **180**, 323–341.
- Yamburenko, M.V., Zubo, Y.O., Vankova, R., Kusnetsov, V.V., Kulaeva, O.N. and Borner, T. (2013) Abscisic acid represses the transcription of chloroplast genes. *J. Exp. Bot.* **64**, 4491–4502.
- Yin, R., Han, K., Heller, W., Albert, A., Dobrev, P.I., Zazimalova, E. and Schaffner, A.R. (2014) Kaempferol 3-O-rhamnoside-7-O-rhamnoside is an endogenous flavonol inhibitor of polar auxin transport in Arabidopsis shoots. *New Phytol.* **201**, 466–475.